Received: 25 April 2021 | Revised: 27 June 2021 | Accepted: 15 July 2021 | Accepted article online: 18 July 2021

DOI: 10.1002/pmic.202100077

Proteomics
Proteomics and Systems Biology

RESEARCH ARTICLE

Current noise of a protein-selective biological nanopore

Jiaxin Sun[1] | Avinash Kumar Thakur[1,2] | Liviu Movileanu[1,3,4]

[1] Department of Physics, Syracuse University, Syracuse, New York, USA

[2] Genentech, Inc., 1 DNA Way, South San Francisco, CA 94080, USA

[3] The BioInspired InstituteSyracuse University, Syracuse, New York, USA

[4] Department of Biomedical and Chemical Engineering, Syracuse University, Syracuse, New York, USA

Correspondence
Liviu Movileanu, Department of Physics, Syracuse University, 201 Physics Building, Syracuse, NY 13244-1130, USA.
Email: lmovilea@syr.edu

Jiaxin Sun and Avinash Kumar Thakur contributed equally to this work.

Funding information
National Institute of General Medical Sciences, Grant/Award Number: R01 GM129429

Abstract

1/*f* current noise is ubiquitous in protein pores, porins, and channels. We have previously shown that a protein-selective biological nanopore with an external protein receptor can function as a 1/*f* noise generator when a high-affinity protein ligand is reversibly captured by the receptor. Here, we demonstrate that the binding affinity and concentration of the ligand are key determinants for the nature of current noise. For example, 1/*f* was absent when a protein ligand was reversibly captured at a much lower concentration than its equilibrium dissociation constant against the receptor. Furthermore, we also analyzed the composite current noise that resulted from mixtures of low-affinity and high-affinity ligands against the same receptor. This study highlights the significance of protein recognition events in the current noise fluctuations across biological membranes.

KEYWORDS
FhuA, ion channel, membrane protein engineering, protein detection, protein dynamics, single-molecule electrophysiology

1 | INTRODUCTION

Nanopores are powerful tools for single-molecule protein identification, detection, and analysis [1–11], suggesting realistic prospects in quantitative proteomics [12–21]. The detection mechanism employs early developments in single-channel electrical recordings [22]. If a single nanopore is located within an insulating membrane and exposed to an electrolytic fluid, then the ionic current traverses the nanopore whenever a voltage bias is applied. Partitioning of either a peptide or a protein into the nanopore occludes the permeation pathway, so that changes in the current signature are noted in the form of transient current blockades. The current amplitude of these blockades, as well as their duration and frequency are at the heart of standard event analysis in single-molecule nanopore detection of proteins. This is the time-domain analysis of single-channel current recordings. An alternative way to analyze these electrical measurements is to inspect the frequency domain using a fast Fourier transformation method. In this manner, the power spectral density (PSD) can be determined, illustrating the distribution and density of statistical current fluctuations acquired at various frequencies.

The nature and amplitude of current noise of both biological [23–38] and synthetic [39–50] nanopores have been extensively examined. Early studies of bacterial porins have revealed the presence of 1/*f* noise in the low-frequency domain with a range of 0–100 Hz [27]. In a logarithmic representation of a PSD diagram, the low-frequency 1/*f* noise denotes a linear increase in the amplitude of current noise by a decrease in the frequency. In general, it is accepted that 1/*f* noise is produced by infrequent and significant fluctuations in the number and local mobility of diffusing charges [51–53]. Moreover, the low-frequency 1/*f* noise is present in many transmembrane pores [33,37,38,50], porins [29,30,32,54–57], and channels [39,58], Yet,

Abbreviations: α, Hooge's phenomenologicalparameter of 1/*f* current noise; ΔI, the absolute difference between the ligand-captured current and ligand-released current; τ_{off}, the ligand-captured time; τ_{on}, the ligand-released time; [L], the ligand concentration; Bn, barnase; Bs, barstar; *c*, the slope of low-frequency 1/*f* current noise in a log-log representation of the PSD; DDM, n-dodecyl-β-D-maltopyranoside; *f*, experimental frequency; f_c, the corner frequency of a Lorentzian fit; f_{cut}, the cut-off frequency, which is the onset frequency of the 1/*f* current noise in the low-frequency domain; f_e, the event frequency in the single-channel electrical trace; FhuA, ferric hydroxamate uptake component A of *Escherichia coli*; f_{min}, the minimum experimental frequency; f_o, the fractional occupancy of the protein receptor by protein ligand; I_{off}, the single-channel current of the ligand-captured substate; I_{on}, the single-channel current of the ligand-released substate; K_D, the equilibrium dissociation constant; k_{off}, the rate constant of dissociation; k_{on}, the rate constant of association; *N*, the number of channels within a membrane; O, adaptor; O_c, the average closed current substate produced by upward current spikes; O_{off}, the ligand-captured current substate; O_{on}, the ligand-released current substate; PSD, the power spectral density; *S*(0), the low-frequency limit of current noise; $S(0)_{max}$, the maximum value of the low-frequency limit of current noise; t-FhuA, a heavily truncated derivative of FhuA

some β-barrel protein pores [23,24,36,59] and porins [31,34] exhibit frequency-independent white noise in the low-frequency regime. We have recently shown that a protein nanopore fused to an external protein receptor exhibits 1/*f* noise whenever reversible captures of a high-affinity protein ligand occurred at the tip of the nanopore [60]. It is worth mentioning that the ligand-captured and ligand-released current substates only showed white noise (e.g., flat noise or frequency independent current noise). Therefore, we concluded that the low-frequency 1/*f* noise was generated during reversible switches between the two current substates of the nanopore.

In this study, we inquired whether the low-frequency 1/*f* current noise of a protein-selective nanopore also depends on the binding affinity of the ligand. Here, the stem of the biological nanopore, simply called t-FhuA (Figure 1A) [61], is the 22-stranded β barrel of ferric hydroxamate uptake component A (FhuA) of *Escherichia coli* [62,63]. We then fused a small 110-residue RNAse barnase (Bn) [64], an external receptor domain, to the N terminus of truncated ferric hydroxamate uptake protein A (t-FhuA) via a Gly/Ser-rich flexible hexapeptide tether. Further, we also covalently attached an unstructured dodecapeptide adaptor (O) to the N terminus of Bn to serve as an external sensing element that changes the single-channel electrical signature of the nanopore upon its transient binding to a protein ligand. This extensive protein engineering facilitated the design and creation of a protein-selective biological nanopore [61], here named Bn-t-FhuA, for the real-time monitoring of protein detection. In a recent study [60], barstar (Bs) [65], a high-affinity 89-residue ligand [66], produced reversible bindings with the tethered Bn receptor, creating the low-frequency 1/*f* noise. In the absence of Bs, Bn-t-FhuA showed a current of ~−50 pA (O_{on}) at a voltage bias of −40 mV (Figure 1B). However, in the presence of Bs, reversible current transitions to a current amplitude of ~−60 pA (O_{off}) were noted (Figure 1C), the frequency of which depended on the Bs concentration [61]. During Bs-released events (O_{on}), it is likely that the O peptide adaptor produced highly frequent and short-lived current spikes of varying amplitude, reaching to an O_c substate. In contrast, during Bs-captured events (O_{off}) such spikes were not present. The high-affinity Bs ligand interacted with Bn-t-FhuA with the rate constant of association, $k_{on} = \sim 1.3 \times 10^7\ M^{-1}\ s^{-1}$, and the rate constant of dissociation, $k_{off} = \sim 0.86\ s^{-1}$, which gave the equilibrium dissociation constant, K_D, of ~64 nM. In the previous work [60], we provided evidence that the magnitude of the 1/*f* noise amplification was strongly dependent on the Bs concentration.

Here, we asked whether the low-frequency 1/*f* noise is generated by a weakly binding protein ligand. This experimental strategy enabled us to examine the PSDs at ligand concentrations much lower than its corresponding equilibrium dissociation constant, K_D, while still generating frequent reversible switches between the two substates of the nanopore. Remarkably, we found that the presence of protein ligand at a concentration much lower than the corresponding K_D no longer creates 1/*f* noise despite frequent reversible switches between the two substates of the nanopore. We then quantitatively compared noise characteristics produced by the low-affinity and high-affinity protein ligands. Finally, we examined the composite effect of a binary mixture of these ligands with different binding affinities.

Statement of significance

Protein and synthetic nanopores represent key elements used in protein detection, identification, and characterization. Electrical recordings of single nanopores have traditionally employed the analysis of time-resolved current fluctuations resulting from their interactions with various protein analytes. An alternative approach of this data processing is inspecting the frequency domain of statistical current fluctuations. Here, we show that a protein-selective biological nanopore exhibits either low-amplitude Lorentzian current noise or high-amplitude 1/*f* current noise. Moreover, we show that a binary mixture of low-affinity and high-affinity protein ligands produces 1/*f* current noise. This outcome is likely determined by the dominant role of the high-affinity protein ligand in creating significant fluctuations in the diffusion of charges through the nanopore.

2 | MATERIALS AND METHODS

2.1 | Cloning and mutagenesis of the protein nanopore and protein ligands

Cloning was performed employing the pPR-IBA1 expression vector [62], The *obn(ggs)$_2$t-fhua* gene encoded the Bn-t-FhuA protein nanopore. This gene encompassed DNA sequences for an extensively t-FhuA [61], a Gly/Serine-rich hexapeptide arm (GGSGGS), a small RNase Bn [64], a dodecapeptide adaptor (MGDRGPEFELGT) [67], as well as *KpnI* sites at both ends [61,68]. Fusion of these polypeptides was conducted at the N terminus of t-FhuA. The overall gene of this modular protein nanopore was created using individual genes of Bn and t-FhuA, *bn* and *t-fhua*, respectively, and assembly PCR reactions. The RNase activity of Bn was suppressed using an H102A mutant of Bn. In this way, Bn-t-FhuA exhibited no toxic activity within the expression host [64,69]. The *bs* gene of the Bs, a high-affinity protein inhibitor of Bn, included a double-alanine mutant, C40A/C82A [70]. The gene that encoded, D39A Bs, a low-affinity protein ligand against Bn, was developed using inverse PCR [68].

2.2 | Protein expression, solubilization, purification, and refolding

Specific methods and protocols for protein expression and purification Bn-t-FhuA were previously described [61,71]. Solubilization of Bn-t-FhuA was performed using 200 mM KCl, 8 M urea, 50 mM Tris-HCl, pH 8 to a concentration of ~15 μM. This solubilization process was conducted for several hours at room temperature. Denatured Bn-t-FhuA samples were refolded by adding n-dodecyl-β-D-maltopyranoside (DDM) to a final concentration of 1.5% (w/v) [72], then slowly dialyzed

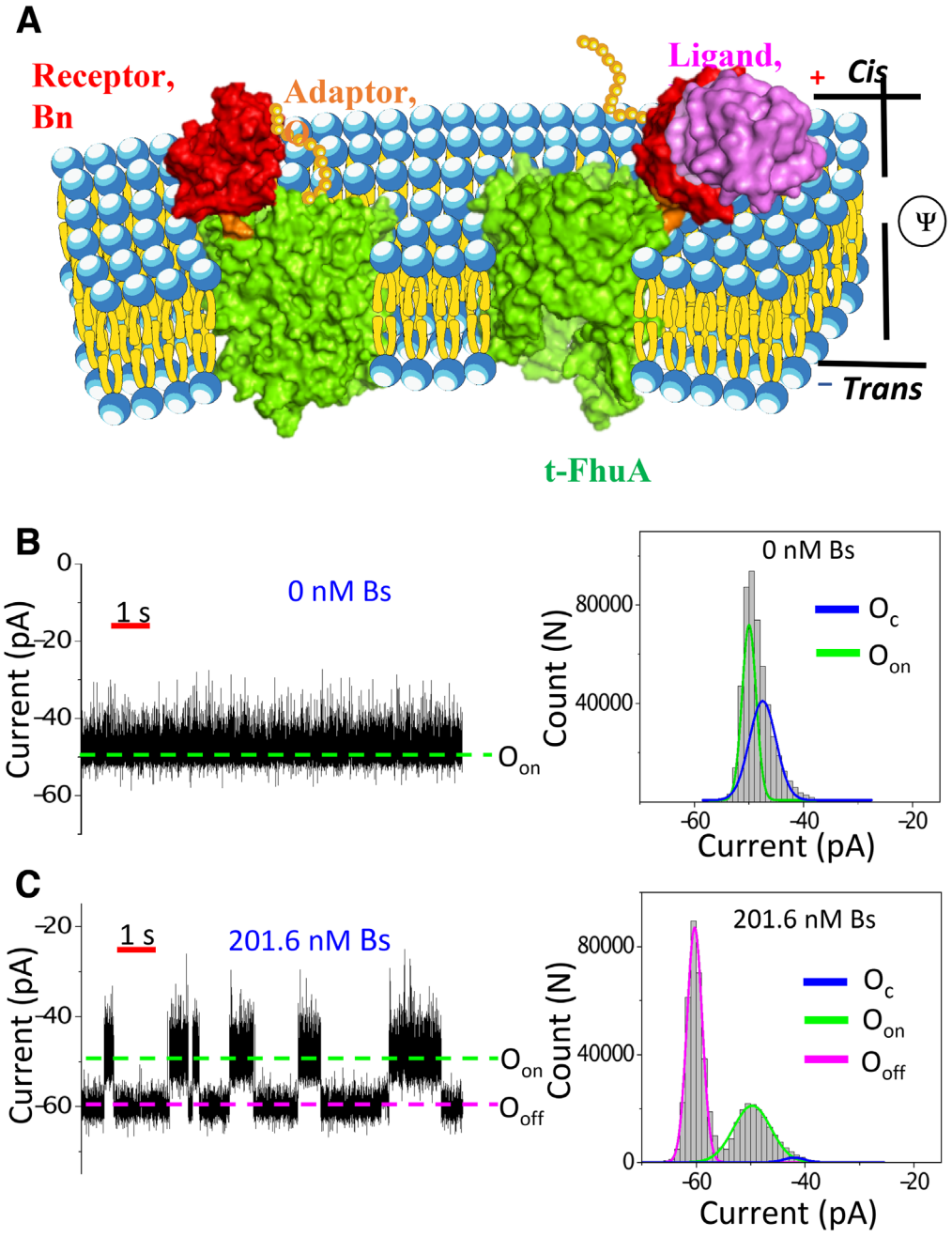

FIGURE 1 Reversible protein ligand captures by a single protein-selective biological nanopore. (A) The composition of a protein-selective biological nanopore, whose scaffold comprises a heavily truncated ferric hydroxamate uptake protein A of *Escherichia coli* (t-FhuA) [61,68]. This outer membrane β-barrel protein pore, which serves as the permeation pathway for ions' transit, was fused to a barnase (Bn) protein receptor via a flexible hexapeptide tether. An unstructured dodecapeptide adaptor (O) was engineered at the N terminus of Bn. Barstar (Bs), a protein ligand, is transiently captured at the tip of this nanopore (Bn-t-FhuA). (B) In the absence of Bs, the open-state current, I_{on}, was −50.0 ± 0.1 pA. The single-channel electrical trace shows upward current spikes, whose residual current, I_c, was −47.5 ± 0.5 pA. (C) Reversible openings of Bn-t-FhuA were noted when 201.6 nM Bs was added to the *cis* side. Here, O_{on} represents the Bs-released substate, whereas O_{off} indicates the Bs-captured substate. The open-state currents of the O_{on} (I_{on}) and O_{off} (I_{off}) substates were −49.8 ± 0.2 pA and −60.1 ± 0.1 pA, respectively. The residual current of spikes, I_c, was −42.0 ± 2.2 pA. Current amplitudes of the peaks were provided as mean ± SEM of individual Gaussian fits. The transmembrane potential was −40 mV. Single-channel electrical traces were low-pass filtered at 1 kHz using an 8-pole Butterworth filter. For (B) and (C), all-points histograms of current amplitudes of individual peaks were illustrated on the right side. These histograms were developed using 10 s-duration single-channel electrical traces

against 200 mM KCl, 20 mM Tris-HCl, pH 8, at 4°C for at least 3 days. For single-channel electrical recordings, protein samples were 20-fold diluted in 200 mM KCl, 20 mM Tris-HCl, pH 8, 0.5% DDM. Protein expression and purification of Bs protein ligands, both wild-type and mutants, were previously reported [61,68].

2.3 | Single-channel electrical recordings using planar lipid bilayers

Single-channel electrical traces were recorded using planar lipid membranes [73,74]. The experimental solution contained 300 mM KCl, 10 mM Tris-HCl, pH 8. The sample of protein nanopore was added to the *cis* side of the chamber (Figure 1A), which was grounded. The final concentration of Bn-t-FhuA was in the range of 0.3–1 ng μL^{-1}. Single-channel electrical currents were recorded employing an Axopatch 200B patch-clamp amplifier (Axon Instruments, Foster City, CA, USA) and digitized using a Digidata 1440A acquisition system (Axon Instruments). The applied transmembrane potential was −40 mV. All single-channel electrical traces were sampled at a frequency of 50 kHz and low-pass filtered at 10 kHz using an 8-pole Butterworth filter, model 900B (Frequency Devices, Ottawa, IL, USA). The acquisition and analysis of single-channel electrical recordings were accomplished using pClamp 10.5 software package (Axon Instruments) and Origin 8.5 (OriginLab, Northampton, MA, USA). All electrical traces were acquired at room temperature (23 ± 1°C).

2.4 | Noise analysis of single-channel current recordings

ClampFit 10.5 (pClamp, Axon Instruments) was used to produce individual PSD plots. This process was achieved by employing a built-in power spectrum function, which was applied to single-channel electrical traces. In general, 10 s-duration single-channel electrical traces were used for creating PSD plots. Averaged PSDs were obtained using 15 distinct PSDs. These PSDs were acquired using $n = 3$ independently reconstituted nanopores with five PSDs of each nanopore experiment. For noise analysis, all traces were low-pass filtered at a frequency of 10 kHz using an 8-pole Butterworth filter. They were used to obtain average values of low-frequency limit of current noise, $S(0)$ [37,75]. $S(0)$ was acquired using the lowest experimental frequency of the PSD [60]. Average single-channel currents of the ligand-released and ligand-captured substates were determined using Gaussian fits of all-points current amplitude histograms. Such average currents were used to determine the average absolute current differences between the two substates of the nanopore (ΔI). These values were employed to compute the model-dependent $S(0)$ values. For fits of the white noise in the low-frequency domain of the PSD, a Lorentzian function was used:

$$S(f) = \frac{S(0)}{1 + \left(\frac{f}{f_c}\right)^2} \quad (1)$$

where f_c is the corner frequency. For fits of $1/f^c$ noise, a linear function was employed in a log-log representation. These latter fits were executed in the frequency range of (f_{min}, f_{cut}). Here, f_{min} and f_{cut} denote the minimum experimental frequency of the PSD and the cut-off frequency of the $1/f$ current noise, respectively. f_{cut} shows to the onset of the low-frequency $1/f$ noise.

3 | RESULTS AND DISCUSSION

3.1 | Low-affinity ligand does not produce $1/f$ noise at concentrations much lower than the equilibrium dissociation constant

In this work, we examined the nature of current noise produced by D39A Bs, a low-affinity Bs ligand. The low-affinity D39A Bs ligand interacts with Bn-t-FhuA with the rate constant of association, $k_{on} = \sim 0.12 \times 10^7\ M^{-1}\ s^{-1}$, and the rate constant of dissociation, $k_{off} = \sim 281\ s^{-1}$, which give the K_D of ~146 μM [61]. The electrical signature of Bn-t-FhuA in the presence of the low-affinity D39A Bs comprises ligand-captured (O_{off}) and ligand-released (O_{on}) events that undergo closely similar transitions between identical current substates for the high-affinity Bs ligand (Figures 1B,C and 2; Figure S1).

However, the Bs-captured time, τ_{off}, for the high-affinity Bs ligand and low-affinity D39A Bs ligand with the tethered Bn measured ~1.16 s and ~3.5 ms, respectively [61], The low-affinity D39A Bs ligand enabled us to test whether the low-frequency $1/f$ current noise is still detectable at ligand concentrations much lower than its corresponding K_D. At a concentration of 181.7 nM D39A Bs, reversible switches between O_{on} and O_{off} were noted (Figure 2A), representing the interactions of the tethered Bn receptor with the low-affinity D39A Bs ligand. As expected, their frequency increased at elevated ligand concentrations of 362.4 nM (Figure 2B) and 723.4 nM (Figure 2C). The supplementary single-channel electrical trace, which was presented at the bottom of Figure 2, shows three such examples of very short-lived current transitions produced by the low-affinity D39A Bs ligand. Moreover, the all-points histograms of current amplitudes on the right side of Figure 2 showed an additional peak, whose substate was named O_c. The current transitions between O_{on} to O_c were likely produced by flickering fluctuations of the O peptide adaptor, while the nanopore dwelled on the D39A Bs-released O_{on} blocked substate. Although the amplitude of this O_c peak fluctuated from trace to trace due to the stochasticity of this process, the amplitude of the O_{off} peak was amplified at increasing D39A Bs concentrations. We have never observed current transitions between the D39A Bs-captured O_{off} open substate and O_c substate. In a previous study [60], we have documented that in the O_{on} substate, which included transitions to and from O_c substate, the nanopore exhibits a high-frequency current noise, but no low-frequency $1/f$ current noise.

Next, we employed noise analysis to generate the PSD (Materials and Methods) of Bn-t-FhuA in the presence of the low-affinity D39A Bs ligand at various concentrations. Surprisingly, we found that the low-frequency $1/f$ current noise is absent under these conditions

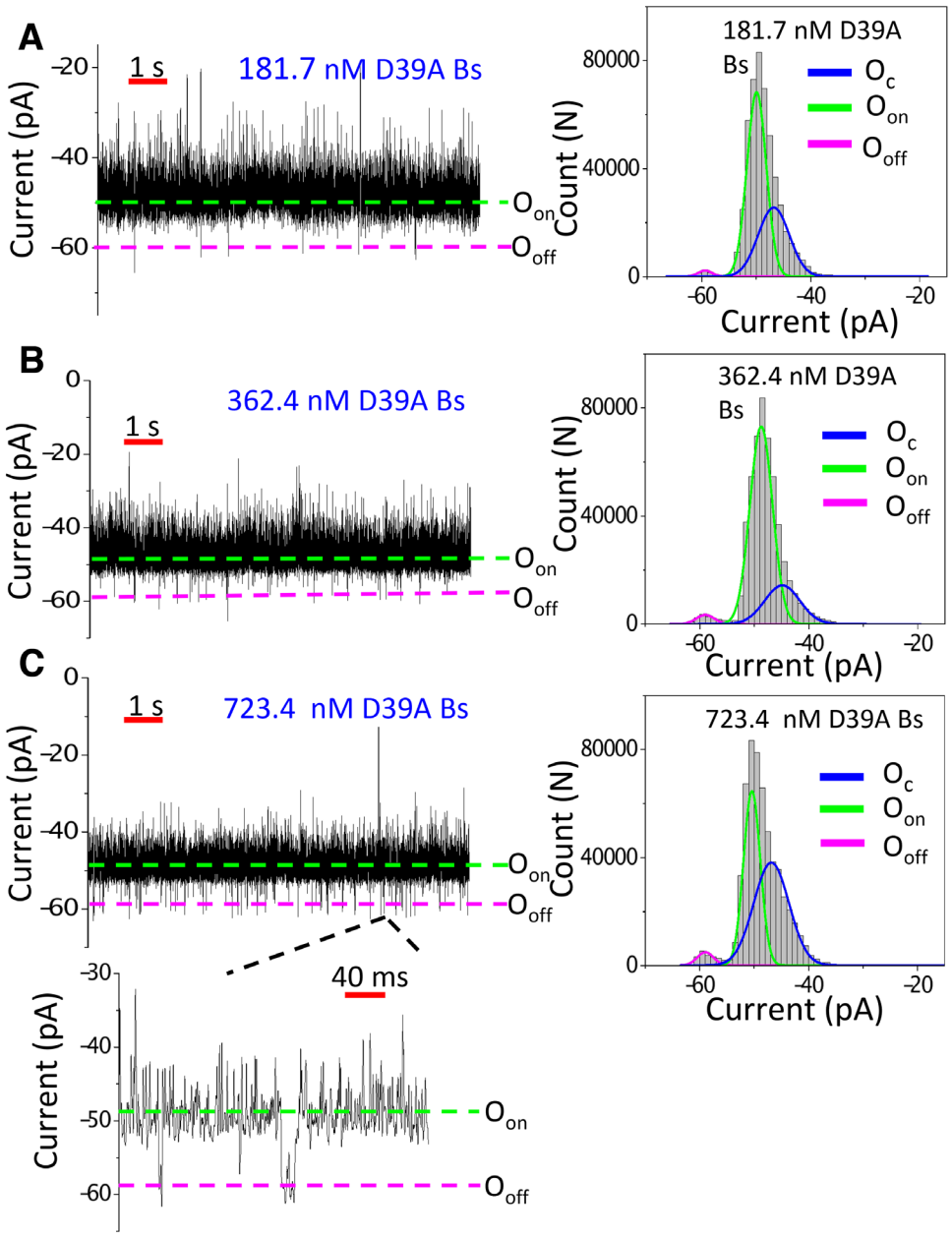

FIGURE 2 Detection of a weakly binding protein ligand by a single protein-selective biological nanopore. The weakly-interacting D39A Bs ligand was added to the *cis* compartment. O_{on} represents the Bs-released open substate, whereas O_{off} indicates the Bs-captured open substate. (A) At 181.7 nM D39A Bs, Ion, Ioff, and Ic were −50.0 ± 0.1 pA, −59.4 ± 0.7 pA, and −46.8 ± 1.5 pA, respectively. (B) At 362.4 nM D39A Bs, Ion, Ioff, and Ic were −48.7 ± 0.2 pA, −59.0 ± 0.7 pA, and −44.9 ± 4.0 pA, respectively. (C) At 723.4 nM D39A Bs, Ion, Ioff, and Ic were −50.4 ± 0.1 pA, −58.9 ± 0.5 pA, and −46.3 ± 0.5 pA, respectively. Current amplitudes of the peaks were provided as mean ± SEM of individual Gaussian fits. The additional trace in (C) shows examples of brief D39A Bs capture events. The transmembrane potential was −40 mV. The single-channel electrical traces were low-pass filtered at 1 kHz using an 8-pole Butterworth filter. All-points histograms of current amplitudes of individual peaks were illustrated on the right side of the figure. These histograms were developed using 10 s-duration single-channel electrical traces

(Figure 3). Therefore, reversible switches no longer generated 1/*f* current noise despite their high probability (Figure 2). In this article, the low-frequency limit of current noise, *S*(0), is the current noise amplitude that corresponds to the lowest experimentally measured frequency of the PSD. We determined the background noise of Bn-t-FhuA at a zero transmembrane potential and in the absence of D39A Bs. This value was $\sim 10^{-29}$ A^2 Hz^{-1}, which is in a good accord with the calculated total background noise. This zero-voltage and ligand-free background noise includes both the Johnson-Nyquest thermal noise [29,49,76–80] of 2.0×10^{-29} A^2 Hz^{-1} and the shot noise [29,49,78–80] of 1.6×10^{-29} A^2 Hz^{-1}. Our calculations were achieved using a single-channel conductance of ~1.26 nS for Bn-t-FhuA [60]. We noted a three-order of magnitude increase in *S*(0), to a value of $\sim 10^{-26}$ A^2 Hz^{-1}, when a transmembrane potential of −40 mV was applied.

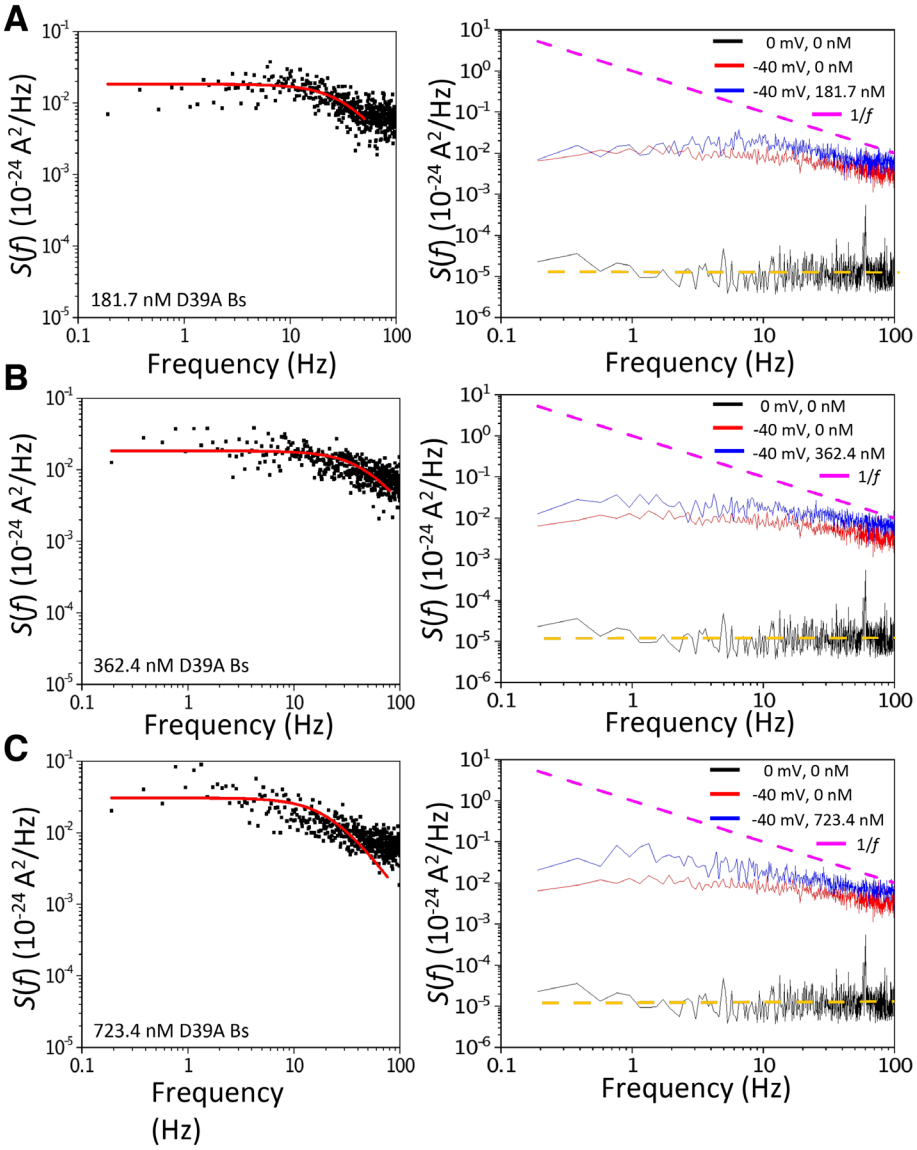

FIGURE 3 Power spectral density (PSD) of single-channel current noise of Bn-t-FhuA recorded at different D39A Bs concentrations. Representative PSDs of single-channel current noise were recorded at different D39A Bs concentrations, as follows: (A) 181.4, (B) 362.4, and (C) 723.4 nM. PSDs were obtained using 15 distinct PSDs. These PSDs were acquired using $n = 3$ independently reconstituted nanopores with five PSDs of each nanopore experiment. Corresponding Lorentzian spectral fits (Materials and Methods) were displayed on the left side. Here, the minimum analyzed frequency, f_{min}, was 0.19 Hz. The corner frequency, f_c, for the three D39A concentrations were the following: (A) 35.0 ± 1.9 Hz, (B) 49.7 ± 2.0 Hz, and (C) 22.3 ± 1.2 Hz. These values were provided as mean ± SEM from individual Lorentzian fits (Materials and Methods). The lower dashed line is the background noise (~2.06 ×10^{-29} A^2 Hz^{-1}), which was computed using Johnson-Nyquist noise function [76,77]

At a concentration of 181.7 nM D39A Bs, we noted a flat Lorentzian noise at frequencies in the range of 0–100 Hz, a low-frequency domain that is characteristic to 1/*f* noise [50] (Figure 3A). A flat noise was also observed at higher D39A Bs concentrations of 362.4 nM (Figure 3B) and 723.4 nM (Figure 3C). In addition, we represented the hypothetical 1/*f* noise lines on the right panels of Figure 3 to highlight the absence of such a noise signature in the low-frequency domain. Recently, we have shown that the amplification in low-frequency 1/*f* noise by a protein ligand of a protein-selective biological nanopore is determined at least in part by reversible switches between ligand-captured and ligand-released substates [60]. Here, our experiments with the low-affinity D39A Bs ligand suggest that the reversible switches are not sufficient for the generation of this noise signature.

3.2 | Quantitative analysis of the white noise produced by the low-affinity protein ligand

A detailed analysis of the noise amplitude in the low-frequency regime revealed that *S*(0) increases by increasing the concentration of the D39A Bs ligand (Figure S2–S4). This outcome was acquired even if we normalized the PSDs to the squared single-channel currents

corresponding to the O_{on} substate, I_{on}^2 (Figure S5). Our finding is not surprising, given that the theoretical prediction of the low-frequency limit of current noise, $S(0)$ [23,81,82], obeys Machlup's equation [81]:

$$S(0) = 4(\Delta I)^2 \tau_{off} \frac{\frac{[L]}{K_D}}{\left(1 + \frac{[L]}{K_D}\right)^3} \quad (2)$$

The function (2) reaches the maximum value at a ligand concentration, [L], equal to $K_D/2$. Here, ΔI is the absolute single-channel current difference between the O_{on} and O_{off} substates. $S(0)$ is a biphasic function with respect to its variable, [L]. This means that the function (2) increases when [L] increases up to its corresponding $K_D/2$, yet it decreases when [L] increases beyond $K_D/2$ (Table S1, Figure S6). Using the kinetic rate constants of binding interactions of the low-affinity D39A Bs ligand with Bn-t-FhuA [61], the maximum $S(0)$ value, $S(0)_{max}$, would be 210.8 × 10^{-27} A^2 Hz^{-1} at a ligand concentration of 73 μM D39A Bs.

However, our experimental $S(0)$ values for inspected submicromolar D39A Bs concentrations were much smaller than $S(0)_{max}$. For instance, $S(0)$, in terms of mean ± SD (n = 3 distinct nanopores), was (2.7 ± 1.1) × 10^{-27} A^2 Hz^{-1}, (6.4 ± 1.2) × 10^{-27} A^2 Hz^{-1}, (11.6 ± 3.5) × 10^{-27} A^2 Hz^{-1}, and (17.3 ± 3.0) × 10^{-27} A^2 Hz^{-1} at D39A Bs concentrations of 90.7 nM, 181.4 nM, 362.4 nM, and 723.4 nM, respectively (Figures S4 and S6, Table S2). This outcome is likely because these concentrations of the low-affinity D39A Bs ligand are at least two orders of magnitude lower than the $K_D/2$. Furthermore, no 1/f noise was noted within this concentration regime despite the presence of numerous reversible switches between the D39A Bs-captured and D39A Bs-released substates. Here, in light of the outcomes of our previous publication [60], we tentatively interpret that these ligand-induced reversible current switches are required, but not sufficient, to generate the low-frequency 1/f noise of a protein-selective biological nanopore (Figure 1A).

To test this interpretation, we next examined the ligand-induced current noise of E76A Bs, a medium-affinity ligand for Bn, whose measured K_D was ~1.06 μM (Figure S7, Table S3). In this case, we added 100 nM E76A Bs to the *cis* side of the chamber. This ligand concentration was a five-fold lower concentration than its corresponding $K_D/2$. Therefore, [L] was in the same order of magnitude with the $K_D/2$. In accord with our interpretation, Bn-t-FhuA showed a signature of low-frequency 1/f noise in these conditions (Figure S8, Table S4). In other words, the fractional occupancy of the Bn receptor by the medium-affinity E76A Bs ligand, f_0, was within the same order of magnitude with the expected fractional occupancy reached in the presence of $K_D/2$ concentration of the ligand. For example, if [L] = $K_D/2$, then the ligand-released time is $\tau_{on} = 2\tau_{off}$, because $K_D = ([L]\tau_{on}/\tau_{off})$. This means that the fractional occupancy, which is defined by $f_o = \tau_{off}/(\tau_{on} + \tau_{off})$, is 33.3%. At [L] values of a 5-fold and a 100-fold lower concentration than the $K_D/2$, f_o is ~9.1% and ~0.5%, respectively. Our interpretation is also consistent with a prior study in which high concentrations, in the low-micromolar range, of the high-affinity Bs produced Lorentzian noise in the low-frequency domain of the PSD [60], In this case, [L] was much higher than its corresponding $K_D/2$.

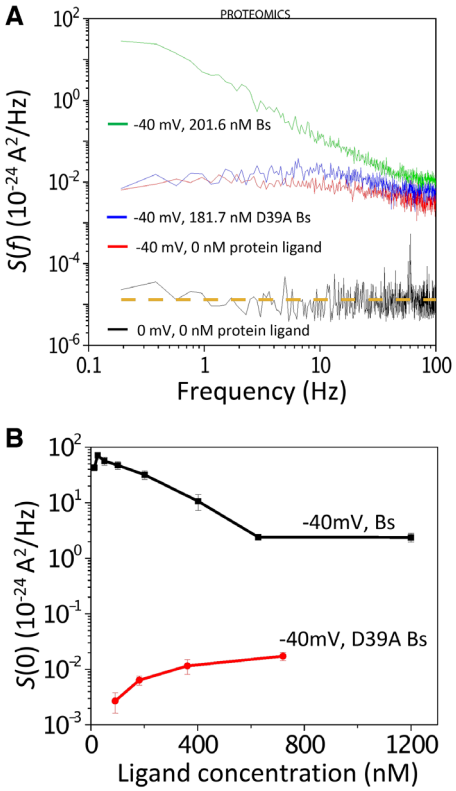

FIGURE 4 Comparison of the excess spectral density of current noise of the Bn-t-FhuA nanopore in the presence of different protein ligands. (A) PSDs that corresponded to single-channel electrical traces, which were either collected at a Bs ligand concentration of 201.6 nM or collected at a D39A Bs ligand concentration of 181.7 nM. (B) Concentration dependence of the current noise produced by either the weakly binding D39A Bs ligand or by the strongly binding Bs ligand. Data points show mean ± SD obtained from n = 3 independently reconstituted nanopores

3.3 | Comparison of current noise produced by the low-affinity and high-affinity protein ligands

Next, we quantitatively compared and contrasted the noise signatures of Bn-t-FhuA under closely similar conditions, but either in the presence of high-affinity or low-affinity protein ligands. Figure 4A shows the averaged PSDs of the background and baseline current noise, which were recorded at zero transmembrane potential and at −40 mV, respectively, both of which in the absence of the protein ligand. Remarkably, at ligand concentrations near to each other, 181.7 nM D39A Bs and 201.6 nM Bs produced signatures of low-amplitude white current noise and high-amplitude 1/f noise, respectively. This distinction in the signature and amplitude of current noise appeared despite frequent ligand-induced reversible switches between the ligand-captured and ligand-released substates in the presence of 181.7 nM D39A Bs (Figure 2A). These concentrations of the low-affinity D39A Bs and high-affinity Bs ligands were 787-fold lower and 3.2-fold higher than their K_D values, respectively. On the other hand, at 723.4 nM D39A Bs, the event frequency, f_e, was ~1.4 s^{-1}. Yet, at 201.6 nM Bs, f_e was ~1.6 s^{-1}. Although f_e values were almost

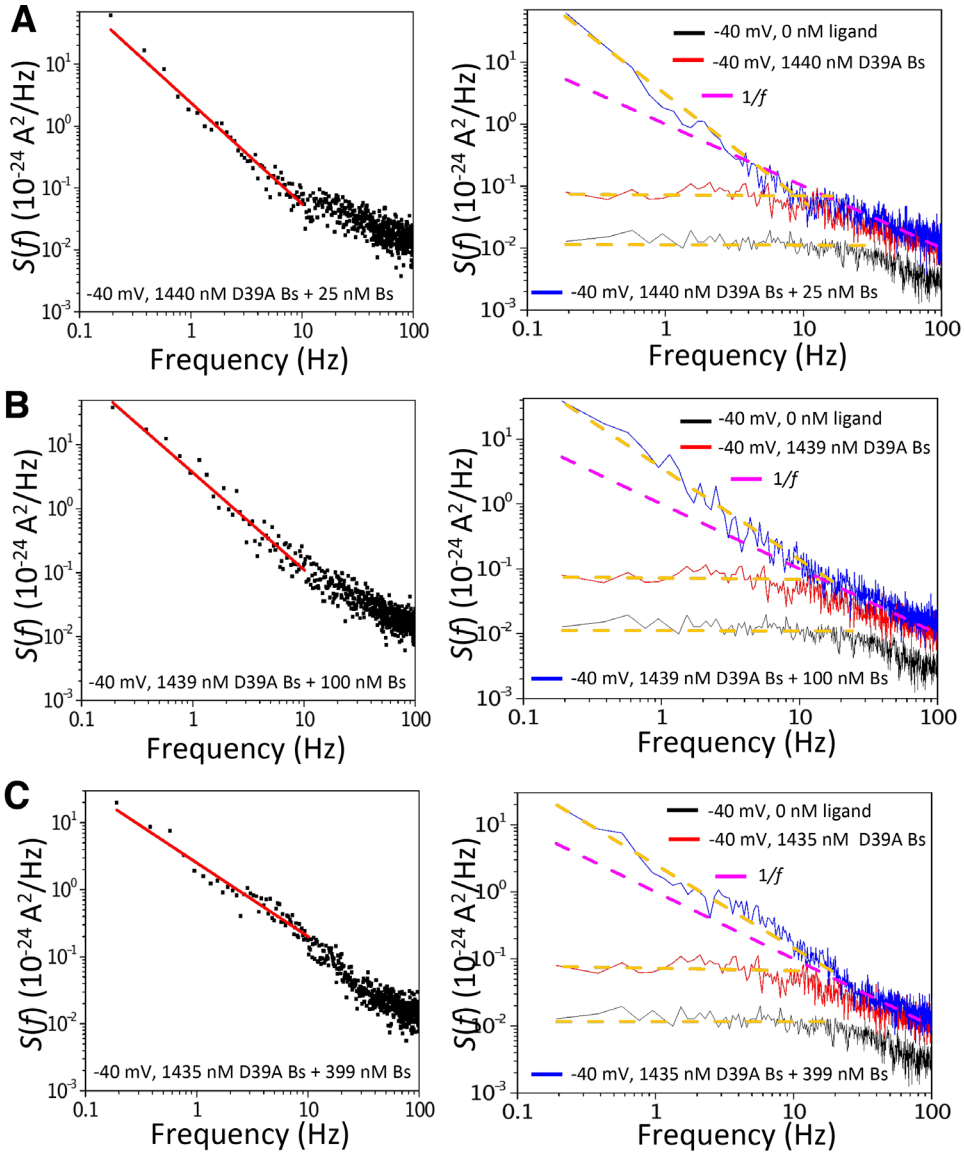

FIGURE 5 The low-frequency domain of current noise determined for binary mixtures comprising high- and low-affinity protein ligands. Representative low-frequency domain PSDs of single-channel current noise recorded in the presence of different binary mixtures, as follows: (A) 1440 nM D39A Bs and 25 nM Bs, (B) 1439 nM D39A Bs and 100 nM Bs, and (C) 1435 nM D39A Bs and 399 nM Bs. The lower dashed line is the baseline current noise acquired at a transmembrane potential of −40 mV. Corresponding linear fits were displayed on the left side for data points in the range of 0.19–10.07 Hz. At a Bs concentration of 25, 100, and 399 nM, the linear slope, *c*, was 1.64 ± 0.05, 1.52 ± 0.06, and 1.10 ± 0.04, respectively. These values were provided as mean ± SEM of linear fits of *S*(*f*) in a logarithmic representation

identical in these cases, the low-affinity D39A Bs ligand produced low-amplitude white noise (Figure 3C), whereas the high-affinity Bs ligand created high-amplitude 1/*f* noise (Figure 4A) in the low-frequency domain. These quantitative comparisons confirm that f_o of the Bn receptor by the protein ligand is an additional key determinant in the amplification of the low-frequency 1/*f* noise.

S(0) of Bn-t-FhuA in the presence of 201.6 nM Bs, in terms of mean ± SD ($n = 3$), was $(31.8 \pm 5.5) \times 10^{-24}$ A^2 Hz^{-1}. This noise amplification is over three orders of magnitude greater than *S*(0) acquired at 181.7 nM D39A Bs ($(6.4 \pm 1.2) \times 10^{-27}$ A^2 Hz^{-1}, $n = 3$) (Table S2). This *S*(0) value for Bs is in accordance with the model-dependent *S*(0) of $\sim 20.5 \times 10^{-24}$ A^2 Hz^{-1} (Equation 2), which was calculated using the kinetic rate constants of the Bn-Bs binding interactions under these experimental conditions [61]. Here, the Bs-amplified 1/*f* noise exhibited a cut-off frequency, f_{cut}, of 50.54 Hz, indicating that this noise signature occurred in the range of 0–100 Hz. Yet, the dependence of *S*(*f*) on the experimental frequency was sharper than 1/*f*. This suggests that the low-frequency domain of *S*(*f*) undergoes a $1/f^c$ dependence [39], with a slope, *c*, in terms of mean ± SEM, of 1.49 ± 0.02 in a logarithmic representation of the PSD.

Figure 4B presents the dependence of *S*(0) on the ligand concentration. It should be noted that *S*(0) is strongly dependent on the high-affinity Bs concentration in a submicromolar range. In contrast, *S*(0) is weakly dependent on the low-affinity D39A Bs concentration under

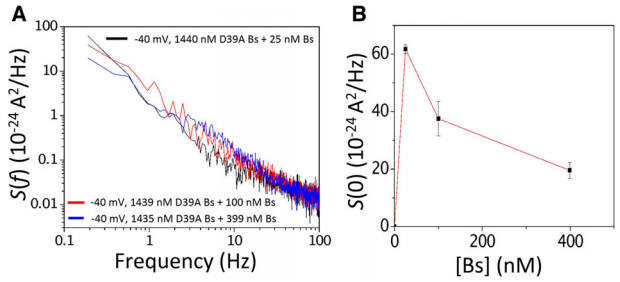

FIGURE 6 The excess spectral density of current noise recorded with binary mixtures of high- and low-affinity protein ligands. (A) Representative PSDs acquired at different Bs ligand concentrations and superimposed on each other. (B) $S(0)$ was acquired at different Bs ligand concentrations. $S(0)$ was the following: (i) $(61.8 \pm 1.5) \times 10^{-24}$ A^2 Hz^{-1} at 1440 nM D39A Bs and 25 nM Bs, (ii) $(37.5 \pm 6.0) \times 10^{-24}$ A^2 Hz^{-1} at 1439 nM D39A Bs and 100 nM Bs, and (iii) $(19.6 \pm 2.7) \times 10^{-24}$ A^2 Hz^{-1} at 1435 nM D39A Bs and 399 nM Bs. $S(0)$ values were provided as mean ± SD using $n = 3$ independently reconstituted nanopores

similar conditions. Again, the magnitude of $S(0)$ for the low-affinity D39A Bs ligand was between two and four orders of magnitude smaller than that value corresponding to the high-affinity Bs ligand.

3.4 | Composite noise of binary mixtures containing the low-affinity and high-affinity ligands

Based on the results obtained above, we questioned the effect of the concurrent presence of the low-affinity and high-affinity Bs ligands on the amplitude and signature of current noise. Therefore, the PSDs of Bn-t-FhuA were examined in the presence of binary mixtures of weakly-interacting D39A Bs and strongly-interacting Bs. In these binary mixtures, the concentration of the low-affinity D39A Bs was maintained at a value of 1.4 μM, whereas the concentration of the high-affinity Bs was changed in a range of 0–400 nM. In this way, we mixed ligands that either produce low-amplitude white current noise or high-amplitude 1/*f* current noise. Under these experimental conditions, we noted the coexistence of the D39A Bs-induced short-lived and Bs-induced long-lived current transitions (Figure S9). Notably, the coexistence of the low-affinity and high-affinity ligands in solution produced low-frequency 1/*f* noise, suggesting the dominant role of the strongly binding protein in the magnitude and signature of current noise (Figures 5 and 6A).

In addition, $S(0)$ depended on the concentration of the high-affinity Bs ligand as one would expect for a strongly interacting protein ligand, according to Machlup's equation (Equation 2) (Figure 6B; Figure S10). For example, the highest $S(0)$, in terms of mean ± SD ($n = 3$), of $(61.8 \pm 1.5) \times 10^{-24}$ A^2 Hz^{-1} was obtained at 25 nM Bs, a ligand concentration slightly lower than the corresponding $K_D/2$ of 32 nM [61]. At 100 nM Bs and 399 nM Bs, the corresponding $S(0)$ values, shown as mean ± SD ($n = 3$), decreased to $(37.5 \pm 6.0) \times 10^{-24}$ A^2 Hz^{-1} and $(19.6 \pm 2.7) \times 10^{-24}$ A^2 Hz^{-1}, respectively (Table S5). This outcome was not changed even if we normalized the PSDs to the squared single-channel currents corresponding to the O_{on} substate, $I_{on}{}^2$ (Figure S11). In addition, these $S(0)$ values compared well with the corresponding values acquired in the presence of the same Bs concentrations, yet in the absence of the low-affinity D39A Bs ligand [60]. Moreover, the cut-off frequency, f_{cut}, namely the onset frequency at which 1/*f* current noise occurs in the low-frequency regime, also depended on the high-affinity Bs concentration. For instance, f_{cut} values at 25, 100, and 399 nM Bs, in terms of mean ± SD ($n = 3$), were 14.3 ± 2.0 Hz, 27.7 ± 3.9 Hz, and 48.5 ± 3.1 Hz, respectively.

The slope of the low-frequency 1/*f* noise also depended on the concentration of the high-affinity Bs ligand. The generalized formula of the low-frequency 1/*f* current noise is the following [27,83–85]:

$$S(f) = \frac{\alpha I_{on}^2}{N f^c} \quad (3)$$

Here, α is Hooge's phenomenological parameter. *f*, *N*, and *c* denote the experimental frequency, number of channels within a membrane, and slope of the low-frequency PSD fit in a logarithmic representation, respectively. We also noted that *c* was over 1 for all examined high-affinity Bs concentrations (Table S5). This is in contrast to other outer membrane proteins, which exhibit intrinsic 1/*f* current noise with a slope, *c*, of ~1 [27,29]. However, a slope different than 1 was noted in other instances [39,41,86]. Furthermore, our α values were in a range close to those previously determined for other β-barrel porins [27].

4 | CONCLUSIONS

In summary, we show that a single protein-selective biological nanopore with an externally engineered protein receptor can either generate low-amplitude white current noise or high-amplitude 1/*f* current noise in the low-frequency domain. This significant distinction in both the magnitude and signature of current noise strongly depends on the fractional occupancy, f_o, of the protein receptor by the protein ligand. At a very low f_o, which corresponds to ligand concentrations much lower than the $K_D/2$, transient ligand-receptor interactions cannot elevate the amplitude of current noise beyond what one would expect for white current noise in the low-frequency domain. However, at a significantly increased f_o, which corresponds to ligand concentrations in the same order of magnitude with the corresponding value of $K_D/2$, reversible switches between the ligand-captured and ligand-released substates produce a significant amplification in the low-frequency 1/*f* current noise. The drawback of time-domain analysis in the form of time-resolved events is the relatively long sampling time, especially in the case of high-affinity protein ligands, which produce long-lived binding events. In the case of low-affinity protein ligands, it is advantageous to determine the concentration of a given sample. The PSDs of 10 s-duration electrical traces can be obtained and analyzed in a matter of minutes, providing a much shorter processing time than one would expect for the analysis of time-resolved events. Finally, we show that competitive binding between the low-affinity and high-affinity ligands against the same Bn receptor produced 1/*f* current noise in a concentration-dependent fashion of the strongly

binding ligand. Our findings agree well with theoretical predictions for the analyte-induced amplification in current noise of protein channels and pores [23,87,88]. With further developments, future explorations of single-molecule protein detection using nanopores may couple the time-domain and frequency-domain analyses of current recordings [30,54].

ACKNOWLEDGMENTS

We thank our colleagues in the Movileanu laboratory for their insightful input and helpful recommendations toward this manuscript as well as their technical assistance during the very early stage of this project. This study was supported by the National Institute of General Medical Sciences of the U.S. National Institutes of Health, grant R01 GM129429 (to L.M.).

CONFLICT OF INTEREST

The authors declare no conflict of interest.

AUTHOR CONTRIBUTIONS

Jiaxin Sun, Avinash Kumar Thakur, and Liviu Movileanu designed research. Jiaxin Sun and Avinash Kumar Thakur performed research and analyzed data. Jiaxin Sun, Avinash Kumar Thakur, and Liviu Movileanu wrote the paper.

DATA AVAILABILITY STATEMENT

The data that support the findings of this study are available from the corresponding author upon reasonable request.

ORCID

Liviu Movileanu https://orcid.org/0000-0002-2525-3341

REFERENCES

1. Rotem, D., Jayasinghe, L., Salichou, M., & Bayley, H. (2012). Protein detection by nanopores equipped with aptamers. *Journal of the American Chemical Society*, *134*(5), 2781–2787.
2. Fahie, M., Chisholm, C., & Chen, M. (2015). Resolved single-molecule detection of individual species within a mixture of anti-biotin antibodies using an engineered monomeric nanopore. *ACS Nano*, *9*(2), 1089–1098.
3. Fahie, M. A., & Chen, M. (2015). Electrostatic interactions between OmpG nanopore and analyte protein surface can distinguish between glycosylated isoforms. *Journal of Physical Chemistry B*, *119*(32), 10198–10206. https://doi.org/10.1021/acs.jpcb.5b06435
4. Fahie, M. A., Yang, B., Mullis, M., Holden, M. A., & Chen, M. (2015). Selective detection of protein homologues in serum using an OmpG nanopore. *Analytical Chemistry*, *87*(21), 11143–11149. https://doi.org/10.1021/acs.analchem.5b03350
5. Lu, B., Stokes, C., Fahie, M., Chen, M., Golovchenko, J. A., & Hau, L. V. (2018). Protein motion and configurations in a form-fitting nanopore: Avidin in ClyA. *Biophysical Journal*, *115*(5), 801–808. https://doi.org/10.1016/j.bpj.2018.07.024
6. Restrepo-Pérez, L., Joo, C., & Dekker, C. (2018). Paving the way to single-molecule protein sequencing. *Nature Nanotechnology*, *13*(9), 786–796. https://doi.org/10.1038/s41565-018-0236-6
7. Restrepo-Pérez, L., Wong, C. H., Maglia, G., Dekker, C., & Joo, C. (2019). Label-free detection of post-translational modifications with a nanopore. *Nano Letters*, *19*(11), 7957–7964. https://doi.org/10.1021/acs.nanolett.9b03134
8. Restrepo-Pérez, L., Huang, G., Bohländer, P. R., Worp, N., Eelkema, R., Maglia, G., Joo, C., & Dekker, C. (2019). Resolving chemical modifications to a single amino acid within a peptide using a biological nanopore. *ACS Nano*, *13*(12), 13668–13676. https://doi.org/10.1021/acsnano.9b05156
9. Huang, G., Willems, K., Bartelds, M., Van Dorpe, P., Soskine, M., & Maglia, G. (2020). Electro-osmotic vortices promote the capture of folded proteins by PlyAB nanopores. *Nano Letters*, *20*(5), 3819–3827. https://doi.org/10.1021/acs.nanolett.0c00877
10. Galenkamp, N. S., Biesemans, A., & Maglia, G. (2020). Directional conformer exchange in dihydrofolate reductase revealed by single-molecule nanopore recordings. *Nature Chemistry*, *12*(5), 481–488. https://doi.org/10.1038/s41557-020-0437-0
11. Zernia, S., Van Der Heide, N. J., Galenkamp, N. S., Gouridis, G., & Maglia, G. (2020). Current blockades of proteins inside nanopores for real-time metabolome analysis. *ACS Nano*, *14*(2), 2296–2307. https://doi.org/10.1021/acsnano.9b09434
12. Mohammad, M. M., & Movileanu, L. (2008). Excursion of a single polypeptide into a protein pore: Simple physics, but complicated biology. *European Biophysics Journal*, *37*(6), 913–925.
13. Bikwemu, R., Wolfe, A. J., Xing, X., & Movileanu, L. (2010). Facilitated translocation of polypeptides through a single nanopore. *Journal of Physics-Condensed Matter*, *22*(45), 454117.
14. Asandei, A., Chinappi, M., Kang, H.-K., Seo, C. H., Mereuta, L., Park, Y., & Luchian, T. (2015). Acidity-mediated, electrostatic tuning of asymmetrically charged peptides interactions with protein nanopores. *ACS Applied Materials & Interfaces*, *7*(30), 16706–16714. https://doi.org/10.1021/acsami.5b04406
15. Asandei, A., Schiopu, I., Chinappi, M., Seo, C. H., Park, Y., & Luchian, T. (2016). Electroosmotic trap against the electrophoretic force near a protein nanopore reveals peptide dynamics during capture and translocation. *ACS Applied Materials & Interfaces*, *8*(20), 13166–13179. https://doi.org/10.1021/acsami.6b03697
16. Asandei, A., Rossini, A. E., Chinappi, M., Park, Y., & Luchian, T. (2017). Protein nanopore-based discrimination between selected neutral amino acids from polypeptides. *Langmuir*, *33*(50), 14451–14459. https://doi.org/10.1021/acs.langmuir.7b03163
17. Chavis, A. E., Brady, K. T., Hatmaker, G. A., Angevine, C. E., Kothalawala, N., Dass, A., Robertson, J. W. F., & Reiner, J. E. (2017). Single molecule nanopore spectrometry for peptide detection. *ACS Sensors*, *2*(9), 1319–1328. https://doi.org/10.1021/acssensors.7b00362
18. Robertson, J. W. F., & Reiner, J. E. (2018). The utility of nanopore technology for protein and peptide sensing. *Proteomics*, *18*(18), 1800026. https://doi.org/10.1002/pmic.201800026
19. Piguet, F., Ouldali, H., Pastoriza-Gallego, M., Manivet, P., Pelta, J., & Oukhaled, A. (2018). Identification of single amino acid differences in uniformly charged homopolymeric peptides with aerolysin nanopore. *Nature Communications*, *9*(1), 966. https://doi.org/10.1038/s41467-018-03418-2
20. Larimi, M. G., Mayse, L. A., & Movileanu, L. (2019). Interactions of a polypeptide with a protein nanopore under crowding conditions. *ACS Nano*, *13*(4), 4469–4477. https://doi.org/10.1021/acsnano.9b00008
21. Ouldali, H., Sarthak, K., Ensslen, T., Piguet, F., Manivet, P., Pelta, J., Behrends, J. C., Aksimentiev, A., & Oukhaled, A. (2020). Electrical recognition of the twenty proteinogenic amino acids using an aerolysin nanopore. *Nature Biotechnology*, *38*(2), 176–181. https://doi.org/10.1038/s41587-019-0345-2
22. Sackmann, B., & Neher, E. (1995). *Single-channel recording* (2nd ed.). New York: Kluwer Academic/Plenum Publishers.
23. Bezrukov, S. M., & Kasianowicz, J. J. (1993). Current noise reveals protonation kinetics and number of ionizable sites in an open protein ion channel. *Physical Review Letters*, *70*(15), 2352–2355.

24. Kasianowicz, J. J., & Bezrukov, S. M. (1995). Protonation dynamics of the alpha-toxin ion channel from spectral analysis of pH-dependent current fluctuations. *Biophysical Journal*, *69*(1), 94–105. https://doi.org/10.1016/s0006-3495(95)79879-4
25. Benz, R., Kolb, H. A., Lauger, P., & Stark, G. (1989). Ion carriers in planar bilayers: relaxation techniques and noise analysis. *Methods in Enzymology*, *171*, 274–286. https://doi.org/10.1016/s0076-6879(89)71017-x
26. Jordy, M., Andersen, C., Schülein, K., Ferenci, T., & Benz, R. (1996). Rate constants of sugar transport through two LamB mutants of *Escherichia coli*: Comparison with wild-type maltoporin and LamB of *Salmonella typhimurium*. *Journal of Molecular Biology*, *259*(4), 666–678.
27. Wohnsland, F., & Benz, R. (1997). 1/f-Noise of open bacterial porin channels. *Journal of Membrane Biology*, *158*(1), 77–85.
28. Bezrukov, S. M., Kullman, L., & Winterhalter, M. (2000). Probing sugar translocation through maltoporin at the single channel level. *Febs Letters*, *476*(3), 224–228.
29. Bezrukov, S. M., & Winterhalter, M. (2000). Examining noise sources at the single-molecule level: 1/f noise of an open maltoporin channel. *Physical Review Letters*, *85*(1), 202–205.
30. Kullman, L., Winterhalter, M., & Bezrukov, S. M. (2002). Transport of maltodextrins through maltoporin: A single-channel study. *Biophysical Journal*, *82*(2), 803–812.
31. Nestorovich, E. M., Rostovtseva, T. K., & Bezrukov, S. M. (2003). Residue ionization and ion transport through OmpF channels. *Biophysical Journal*, *85*(6), 3718–3729.
32. Denker, K., Orlik, F., Schiffler, B., & Benz, R. (2005). Site-directed mutagenesis of the greasy slide aromatic residues within the LamB (maltoporin) channel of *Escherichia coli*: Effect on ion and maltopentaose transport. *Journal of Molecular Biology*, *352*(3), 534–550. https://doi.org/10.1016/j.jmb.2005.07.025
33. Orlik, F., Schiffler, B., & Benz, R. (2005). Anthrax toxin protective antigen: inhibition of channel function by chloroquine and related compounds and study of binding kinetics using the current noise analysis. *Biophysical Journal*, *88*(3), 1715–1724. https://doi.org/10.1529/biophysj.104.050336
34. Danelon, C., Nestorovich, E. M., Winterhalter, M., Ceccarelli, M., & Bezrukov, S. M. (2006). Interaction of zwitterionic penicillins with the OmpF channel facilitates their translocation. *Biophysical Journal*, *90*(5), 1617–1627.
35. Nestorovich, E. M., Karginov, V. A., Berezhkovskii, A. M., & Bezrukov, S. M. (2010). Blockage of anthrax PA63 pore by a multicharged high-affinity toxin inhibitor. *Biophysical Journal*, *99*(1), 134–143.
36. Harrington, L., Cheley, S., Alexander, L. T., Knapp, S., & Bayley, H. (2013). Stochastic detection of Pim protein kinases reveals electrostatically enhanced association of a peptide substrate. *Proceedings of the National Academy of Sciences of the United States of America*, *110*(47), E4417–E4426.
37. Yamini, G., & Nestorovich, E. M. (2017). Relevance of the alternate conductance states of anthrax toxin channel. *Proceedings of the National Academy of Sciences of the United States of America*, *114*(13), E2545–E2546. https://doi.org/10.1073/pnas.1701841114
38. Momben Abolfath, S., Kolberg, M., Karginov, V. A., Leppla, S. H., & Nestorovich, E. M. (2019). Exploring the nature of cationic blocker recognition by the anthrax toxin channel. *Biophysical Journal*, *117*(9), 1751–1763. https://doi.org/10.1016/j.bpj.2019.08.041
39. Siwy, Z., & Fuliński, A. (2002). Origin of 1/f(alpha) noise in membrane channel currents. *Physical Review Letters*, *89*(15), 158101. https://doi.org/10.1103/PhysRevLett.89.158101
40. Tabard-Cossa, V., Trivedi, D., Wiggin, M., Jetha, N. N., & Marziali, A. (2007). Noise analysis and reduction in solid-state nanopores. *Nanotechnology*, *18*(30), 305505.
41. Smeets, R. M. M., Keyser, U. F., Dekker, N. H., & Dekker, C. (2008). Noise in solid-state nanopores. *Proceedings of the National Academy of Sciences of the United States of America*, *105*(2), 417–421.
42. Hoogerheide, D. P., Garaj, S., & Golovchenko, J. A. (2009). Probing surface charge fluctuations with solid-state nanopores. *Physical Review Letters*, *102*(25), 256804.
43. Powell, M. R., Vlassiouk, I., Martens, C., & Siwy, Z. S. (2009). Nonequilibrium 1/f noise in rectifying nanopores. *Physical Review Letters*, *103*(24), 248104. https://doi.org/10.1103/PhysRevLett.103.248104
44. Smeets, R. M. M., Dekker, N. H., & Dekker, C. (2009). Low-frequency noise in solid-state nanopores. *Nanotechnology*, *20*(9), 095501.
45. Tasserit, C., Koutsioubas, A., Lairez, D., Zalczer, G., & Clochard, M.-C. (2010). Pink noise of ionic conductance through single artificial nanopores revisited. *Physical Review Letters*, *105*(26), 260602. https://doi.org/10.1103/PhysRevLett.105.260602
46. Beamish, E., Kwok, H., Tabard-Cossa, V., & Godin, M. (2012). Precise control of the size and noise of solid-state nanopores using high electric fields. *Nanotechnology*, *23*(40), 405301.
47. Heerema, S. J., Schneider, G. F., Rozemuller, M., Vicarelli, L., Zandbergen, H. W., & Dekker, C. (2015). 1/f noise in graphene nanopores. *Nanotechnology*, *26*(7), 074001. https://doi.org/10.1088/0957-4484/26/7/074001
48. Hyland, B., Siwy, Z. S., & Martens, C. C. (2015). Nanopore current oscillations: Nonlinear dynamics on the nanoscale. *Journal of Physical Chemistry Letters*, *6*(10), 1800–1806. https://doi.org/10.1021/acs.jpclett.5b00520
49. Fragasso, A., Pud, S., & Dekker, C. (2019). 1/f noise in solid-state nanopores is governed by access and surface regions. *Nanotechnology*, *30*(39), 395202. https://doi.org/10.1088/1361-6528/ab2d35
50. Fragasso, A., Schmid, S., & Dekker, C. (2020). Comparing current noise in biological and solid-state nanopores. *ACS Nano*, *14*(2), 1338–1349. https://doi.org/10.1021/acsnano.9b09353
51. Hooge, F. N., & Hoppenbrouwers, A. M. H. (1969). Amplitude distribution of 1/f noise. *Physica*, *42*(3), 331–339. https://doi.org/10.1016/0031-8914(69)90027-5
52. Voss, R. F., & Clarke, J. (1976). Flicker (1/f) noise: Equilibrium temperature and resistance fluctuations. *Physical Review B*, *13*(2), 556–573.
53. Hooge, F. N. (1976). 1/f noise. *Physica B & C*, *83*(1), 14–23. https://doi.org/10.1016/0378-4363(76)90089-9.
54. Hilty, C., & Winterhalter, M. (2001). Facilitated substrate transport through membrane proteins. *Physical Review Letters*, *86*(24), 5624–5627.
55. Andersen, C., Cseh, R., Schülein, K., & Benz, R. (1998). Study of sugar binding to the sucrose-specific ScrY channel of enteric bacteria using current noise analysis. *Journal of Membrane Biology*, *164*(3), 263–274.
56. Nekolla, S., Andersen, C., & Benz, R. (1994). Noise analysis of ion current through the open and the sugar-induced closed state of the LamB channel of *Escherichia coli* outer membrane: Evaluation of the sugar binding kinetics to the channel interior. *Biophysical Journal*, *66*(5), 1388–1397. https://doi.org/10.1016/s0006-3495(94)80929-4
57. Andersen, C., Jordy, M., & Benz, R. (1995). Evaluation of the rate constants of sugar–transport through maltoporin (LAMB) of *Escherichia coli* from the sugar-induced current noise. *Journal of General Physiology*, *105*(3), 385–401.
58. Banerjee, J., & Ghosh, S. (2005). Investigating interaction of ligands with voltage dependent anion channel through noise analyses. *Archives of Biochemistry and Biophysics*, *435*(2), 369–371. https://doi.org/10.1016/j.abb.2004.12.019
59. Bezrukov, S. M., Krasilnikov, O. V., Yuldasheva, L. N., Berezhkovskii, A. M., & Rodrigues, C. G. (2004). Field-dependent effect of crown ether (18-crown-6) on ionic conductance of {alpha}-hemolysin channels. *Biophysical Journal*, *87*(5), 3162–3171.
60. Sun, J., Thakur, A. K., & Movileanu, L. (2020). Protein ligand-induced amplification in the 1/f noise of a protein-selective nanopore. *Langmuir*, *36*(50), 15247–15257. https://doi.org/10.1021/acs.langmuir.0c02498

61. Thakur, A. K., & Movileanu, L. (2019). Real-time measurement of protein-protein interactions at single-molecule resolution using a biological nanopore. *Nature Biotechnology*, *37*(1), 96–101. https://doi.org/10.1038/nbt.4316
62. Mohammad, M. M., Howard, K. R., & Movileanu, L. (2011). Redesign of a plugged beta-barrel membrane protein. *Journal of Biological Chemistry*, *286*(10), 8000–8013.
63. Locher, K. P., Rees, B., Koebnik, R., Mitschler, A., Moulinier, L., Rosenbusch, J. P., & Moras, D. (1998). Transmembrane signaling across the ligand-gated FhuA receptor: Crystal structures of free and ferrichrome-bound states reveal allosteric changes. *Cell*, *95*(6), 771–778.
64. Schreiber, G., & Fersht, A. R. (1993). Interaction of barnase with its polypeptide inhibitor barstar studied by protein engineering. *Biochemistry*, *32*(19), 5145–5150.
65. Deyev, S. M., Waibel, R., Lebedenko, E. N., Schubiger, A. P., & Plückthun, A. (2003). Design of multivalent complexes using the barnase*barstar module. *Nature Biotechnology*, *21*(12), 1486–1492. https://doi.org/10.1038/nbt916
66. Buckle, A. M., Schreiber, G., & Fersht, A. R. (1994). Protein-protein recognition: Crystal structural analysis of a barnase-barstar complex at 2.0-A resolution. *Biochemistry*, *33*(30), 8878–8889.
67. Kudlinzki, D., Schmitt, A., Christian, H., & Ficner, R. (2012). Structural analysis of the C-terminal domain of the spliceosomal helicase Prp22. *Biological Chemistry*, *393*(10), 1131–1140. https://doi.org/10.1515/hsz-2012-0158
68. Thakur, A. K., & Movileanu, L. (2019). Single-molecule protein detection in a biofluid using a quantitative nanopore sensor. *ACS Sensors*, *4*(9), 2320–2326. https://doi.org/10.1021/acssensors.9b00848
69. Schreiber, G., & Fersht, A. R. (1995). Energetics of protein-protein interactions: Analysis of the barnase-barstar interface by single mutations and double mutant cycles. *Journal of Molecular Biology*, *248*(2), 478–486.
70. Guillet, V., Lapthorn, A., Hartley, R. W., & Mauguen, Y. (1993). Recognition between a bacterial ribonuclease, barnase, and its natural inhibitor, barstar. *Structure (London, England)*, *1*(3), 165–176.
71. Niedzwiecki, D. J., Mohammad, M. M., & Movileanu, L. (2012). Inspection of the engineered FhuA deltaC/delta4L protein nanopore by polymer exclusion. *Biophysical Journal*, *103*(10), 2115–2124.
72. Wolfe, A. J., Si, W., Zhang, Z., Blanden, A. R., Hsueh, Y.-C., Gugel, J. F., Pham, B., Chen, M., Loh, S. N., Rozovsky, S., Aksimentiev, A., & Movileanu, L. (2017). Quantification of membrane protein-detergent complex interactions. *Journal of Physical Chemistry B*, *121*(44), 10228–10241. https://doi.org/10.1021/acs.jpcb.7b08045
73. Liu, J., Eren, E., Vijayaraghavan, J., Cheneke, B. R., Indic, M., Van Den Berg, B., & Movileanu, L. (2012). OccK channels from *Pseudomonas aeruginosa* exhibit diverse single-channel electrical signatures, but conserved anion selectivity. *Biochemistry*, *51*(11), 2319–2330.
74. Couoh-Cardel, S., Hsueh, Y.-C., Wilkens, S., & Movileanu, L. (2016). Yeast V-ATPase proteolipid ring acts as a large-conductance transmembrane protein pore. *Scientific Reports*, *6*, 24774. https://doi.org/10.1038/srep24774
75. Bezrukov, S. M., Liu, X., Karginov, V. A., Wein, A. N., Leppla, S. H., Popoff, M. R., Barth, H., & Nestorovich, E. M. (2012). Interactions of high-affinity cationic blockers with the translocation pores of *B. anthracis*, *C. botulinum*, and *C. perfringens* binary toxins. *Biophysical Journal*, *103*(6), 1208–1217. https://doi.org/10.1016/j.bpj.2012.07.050
76. Johnson, J. B. (1928). Thermal agitation of electricity in conductors. *Physical Review*, *32*, 97–109.
77. Nyquist, H. (1928). Thermal agitation of electric charge in conductors. *Physical Review*, *32*, 110–113.
78. Sherman-Gold, R. (1993). Noise in electrophysiological measurements. In R. Sherman-Gold (Ed.), *The Axon Guide*, (pp. 235–263), Chapter 12. Axon Instruments, Inc.
79. Benndorf, K. (1995). Low-noise recording. In B. Sakmann & E. Neher (Eds.), *Single-channel recoring* (2nd ed., pp. 129–153). New York, NY: Plenum Press.
80. Uram, J. D., Ke, K., & Mayer, M. (2008). Noise and bandwidth of current recordings from submicrometer pores and nanopores. *ACS Nano*, *2*(5), 857–872. https://doi.org/10.1021/nn700322m
81. Machlup, S. (1954). Noise in semiconductors: Spectrum of a two-parameter random signal *Journal of Applied Physics*, *25*(3), 341–343. https://doi.org/10.1063/1.1721637
82. Rostovtseva, T. K., Komarov, A., Bezrukov, S. M., & Colombini, M. (2002). VDAC channels differentiate between natural metabolites and synthetic molecules. *Journal of Membrane Biology*, *187*(2), 147–156.
83. Hooge, F. N., Kleinpenning, T. G. M., & Vandamme, L. K. J. (1981). Experimental studies on 1/f noise. *Reports on Progress in Physics*, *44*(5), 479–532. https://doi.org/10.1088/0034-4885/44/5/001
84. Hooge, F. N. (1972). Discussion of recent experiments on 1/f noise. *Physica*, *60*(1), 130–144. https://doi.org/10.1016/0031-8914(72)90226-1
85. Hooge, F. N. (1969). 1/f noise is no surface effect. *Physics Letters A*, *29*(3), 139–140. https://doi.org/10.1016/0375-9601(69)90076-0
86. Hooge, F. N. (1970). 1/f noise in the conductance of ions in aqueous solutions. *Physics Letters A*, *33*(3), 169–170. https://doi.org/10.1016/0375-9601(70)90713-9
87. Bezrukov, S. M., & Kasianowicz, J. J. (1997). The charge state of an ion channel controls neutral polymer entry into its pore. *The European Biophysics Journal*, *26*(6), 471–476.
88. Rostovtseva, T. K., Komarov, A., Bezrukov, S. M., & Colombini, M. (2002). Dynamics of nucleotides in VDAC channels: Structure-specific noise generation. *Biophysical Journal*, *82*(1 Pt 1), 193–205. https://doi.org/10.1016/s0006-3495(02)75386-1

SUPPORTING INFORMATION

Additional supporting information may be found online https://doi.org/10.1002/pmic.202100077 in the Supporting Information section at the end of the article.

How to cite this article: Sun, J., Thakur, A. K., & Movileanu, L. (2022). Current noise of a protein-selective biological nanopore. *Proteomics*, *22*, e2100077. https://doi.org/10.1002/pmic.202100077